



# Valorization of Hemp Stalk Waste Through Thermochemical Conversion for Energy and Electrical Applications

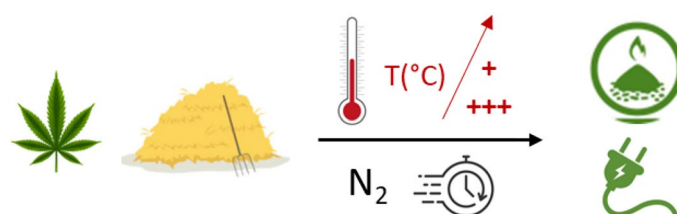
Laetitia Marrot<sup>1,2</sup> · Kevin Candelier<sup>3,4</sup> · Jérémy Valette<sup>3,4</sup> · Charline Lanvin<sup>3,4</sup> · Barbara Horvat<sup>5</sup> · Lea Legan<sup>6</sup> · David B. DeVallance<sup>1,2</sup>

Received: 6 June 2021 / Accepted: 11 November 2021 / Published online: 27 November 2021  
© The Author(s) 2021

## Abstract

The presented research aimed at finding new ways to value hemp by-products (stalks) from the cannabidiol industry through thermochemical conversion. Chemical and elemental composition of hemp biomass was investigated by successive chemical extractions and Scanning Electron Microscopy along with Energy-dispersive X-ray Spectroscopy. Proximate and elemental analyses completed the chemical characterization of the hemp biomass and its biochar. Thermogravimetric analysis of the hemp biomass allowed to understand its kinetic of decomposition during thermal conversion. The carbon structure and porosity of the biochar were assessed by Raman spectroscopy and CO<sub>2</sub> gas adsorption. Properties of interest were the energy production measured through calorific values, and the electrical conductivity. Two ways of valorisation of the hemp biomass were clearly identified, depending mainly on the chosen pyrolysis temperature. Hemp biochar carbonized at 400–600°C were classified as lignocellulosic materials with a good potential for solid biofuel applications. Specifically, the resulting carbonized biochar presented low moisture content (below 2.50%) favourable for high fuel quality, low volatile matter (27.1–10.4%) likely to show lower particle matter emissions, limited ash content (6.8–9.8%) resulting in low risk of fouling issues during the combustion, high carbon content (73.8–86.8%) suggesting strong energy density, associated with high higher heating values (28.45–30.95 MJ kg<sup>-1</sup>). Hemp biochar carbonized at 800–1000 °C displayed interesting electrical conductivity, opening opportunities for its use in electrical purposes. The electrical conductivity was related to the evolution of the biochar microstructure (development of graphite-like structure and changes in microporosity) in regard with the thermochemical conversion process parameters.

## Graphical abstract



**Keywords** Hemp · Pyrolysis · Carbonization · Thermal conversion · Higher heating value · Energy · Biochar · Electrical conductivity

## Statement of Novelty

Most hemp carbonization processes currently focus on biochar for lower-value applications (e.g., soil amendment); however, there is growing interest in using by-products (i.e., stalks) from cannabidiol (CBD) oil production for

✉ Laetitia Marrot  
laetitia.marrot@innorenew.eu

Extended author information available on the last page of the article

higher-value applications related to solid biofuels and bio-composites. The present study assessed the potential of hemp valorization through pyrolysis conversion to obtain solid biofuel and electrically conductive materials for bio-composites. Different applications can be targeted according to the pyrolysis intensity: solid biofuels with pyrolysis performed at low intensity and electrically conductive carbon materials through high temperature pyrolysis. Through thermal conversion, hemp can be transformed into electrically conductive materials with a very high fixed carbon content and an organized carbon structure for potential applications as battery electrodes, composites, and sensor applications.

## Introduction

Hemp (*Cannabis sativa* L.) is an annual plant that grows under various climate and soil conditions. Hemp cultivation is possible between the 25th and 55th parallel, north and south, which represents almost every continent. Hemp fits well in a crop rotation by providing good soil structure, elimination of competing weeds and the ability to withstand pests without the use of high levels of pesticides and insecticides. Additionally, the required calcium and water to grow hemp are usually found in sufficient levels naturally, and supplementation, when needed, is relatively low [1]. The hemp plant is quite versatile, and all parts can be used for different applications [2]. In Slovenia and most Western European countries, hemp is primarily grown for producing cannabidiol (CBD) oil extracted from the flowers and leaves. The remaining hemp by-products, i.e. the stalks, including fibres and shives, represent about 70% of the plant's dried weight [1] and are likely to end up as low-value products or waste.

Due to a fast growth rate, high amount of biomass and promising energy output-to-input ratios, hemp is considered a potentially valuable energy crop [3]. Hemp's solid fuel properties are similar to those of woody biomass (i.e., willow) and higher than those of cereal straw, miscanthus and reed canary grass grown in the same region [4]. However, agronomical practices, such as harvesting period, have been shown to impact hemp's combustion-related fuel properties [4]. In a recent review, Parvez et al. [5] identified a lack of research on the thermochemical conversion of industrial hemp as a major challenge that prevents the wide use of hemp as fuel materials. Indeed, some technical challenges linked with the intrinsic properties of raw biomass hinder their direct use in energy production systems. Specifically, untreated hemp biomass displays a very fibrous outer structure that poses difficulties in grinding, and then requires additional energy for the grinding process [6]. Raw biomass generally contains a higher moisture content and amount of volatile matter, which reduces the thermal efficacy and

increases air pollutant emissions [7]. Finally, biomass materials contain alkali-alkaline earth metals and halogens that can cause fouling, slagging or corrosion issues in the boiler during operation [8]. Recently, Nunes et al. [9] reported that energy densification through thermochemical conversion and physical densification of agricultural by-products (coconut shells, sugarcane bagasse, cashew nutshells and palm kernel shells) can provide suitable fuel replacements for coal in energy production from both a logistics and heating standpoint.

Thermochemical conversion technologies such as torrefaction or pyrolysis (carbonization) assist in reducing deterioration of biomass by microorganisms during storage [10] and improve biomass fuel properties (higher energy density, calorific value, carbon content and lower oxygen content) [11–15]. Additionally, thermochemical conversion has been shown to decrease the release of potentially toxic elements by stabilizing them within the resulting solid fuel material (e.g., biochar) [16]. Biochar is an important material for environmental management to mitigate greenhouse gas emissions, such as sequestration of CO<sub>2</sub> and CH<sub>4</sub>, and ozone-depleting N<sub>2</sub>O emissions [17]. In addition, to use as soil amendments and solid fuel, biochar materials produced through thermochemical processes exhibit a diverse range of interesting properties (electrical conductivity, porosity, thermal stability, activated surface area) that make them suitable for innovative integration in coatings, nanomaterials and bio-composites. For example, Wallace et al. [18] investigated reinforcing bio-composites by using biochar produced from hemp straw in E-glass fibre in a vinyl-ester polymer matrix. Nan et al. [19] indicated that the addition of biochar in polyvinyl alcohol/biochar composites increased tensile modulus and storage modulus above the glass transition temperature but reduced the tensile strength, increased the thermal decomposition temperature of the composites, and provided to the composites an electrical conductivity similar to most carbon nanotube and graphene reinforced polyvinyl alcohol composites. The electrical conductivity of biochar, specifically, has attracted attention for the development of batteries [20], supercapacitors [21, 22] and pressure sensor materials [23]. Sun et al. [21] reported that bio-based carbon from hemp hurds and bast fibres prepared via hydrothermal processing and chemical activation showed interesting specific capacitance and high energy density with good potential for an application as supercapacitor electrodes. Specific capacitance and capacitive retention properties were related to the surface area and fraction of the mesopores induced by the chemical activation. However, the influence of pyrolysis temperature and biochar composition was not considered in their study, and more generally the impact of the process parameters and biochar characteristics impacting the electrical properties remain poorly understood. Given the inherent growing interest in using biomass as a renewable carbon

material source for high-value applications, a better understanding of the processing parameters, such as thermochemical heating rate, pyrolysis temperature and residence time, on the resulting properties will help further the development of biochar from hemp. In this study, various carbonization scenarios of hemp stalks were performed: four pyrolysis temperatures from 400 to 1000 °C, two heating rates (200 °C h<sup>-1</sup> and 2000 °C h<sup>-1</sup>) and two different residence time (30 min and 60 min). The thermal, chemical, physical, energy and electrical properties of hemp stalks enhanced through thermochemical process were investigated for use in biofuel and electrical purposes.

## Materials and Methods

### Chemical Composition of the Raw Hemp Biomass

Hemp stalks (*Cannabis sativa*, dioecious Futura 75 variety) were supplied by the Vrhivšek farm (Frankolovo, Slovenia). The hemp plant was sown in April 2020 and harvested on 29 September 2020. The biochemical composition, as extractives, holocellulose, hemicelluloses, alpha-cellulose (α-cellulose) contents and klason lignin contents, was determined by adapted literature procedures with minor modifications [24]. For each fraction determination, the following steps were triplicated.

#### Extractives Content

To evaluate extractive content, 15 g of hemp stalks were first ground and passed through different sieves to obtain particles ranging between 0.2 and 0.5 mm. These particles were then oven-dried at 103 °C during 24 h and successively washed in a Soxhlet extractor with acetone [Honeywell 32201] (6 h), followed by toluene:ethanol mixture (2:1; v:v) [Honeywell, 34866: Honeywell, 32294] (6 h) and then distilled water (6 h). Between each solvent extraction step, the washed sawdust was oven-dried at 103 °C during 24 h and weighed to determined acetone-extractives content (Ext<sub>ac</sub>%), toluene:ethanol-extractives content (Ext<sub>tol:eth</sub>%), water-extractives content (Ext<sub>H<sub>2</sub>O</sub>%), and then calculated total extractives contents according to the Eq. (1).

$$Ext_{tot}\% = Ext_{ac}\% + Ext_{tol:eth}\% + Ext_{H_2O}\% \quad (1)$$

#### Holocellulose Content

To measure holocellulose content, 500 mg of extracted particles were first placed in a 100 mL flask containing 30 mL of distilled water and heated at 75 °C. Glacial acetic acid [Carlo Erba 524520] (0.1 mL) and 15% aqueous sodium chlorite

[Sigma-Aldrich 244155] (2 mL) were then added each hour for 7 h. The mixture was filtered on a Büchner funnel and the residue washed with water, Soxhlet extracted for 2 h with ethanol and dried at 103 °C to a constant mass (M<sub>holo</sub>, in mg). Holocellulose content was calculated according to the Eq. (2).

$$Holocellulose(\%) = \left[ \frac{M_{holo}}{500 \times (1 + Ext_{tot}\%)} \right] \times 100 \quad (2)$$

#### Hemicelluloses and α-Cellulose Content

The dried holocellulose previously prepared was placed into a glass covered, 250 mL glass beaker containing 10 mL of 17.5% NaOH [Sigma-Aldrich 30620-R] solution that was maintained at 20 °C in a water bath. This mixture was agitated with caution with a rod glass until the holocellulose was soaked with the NaOH solution. After fully soaked, 5 mL of 17.5% NaOH solution were then added every 5 min during 15 min time period and the mixture was left for 30 min. The mixture was then diluted with 33 mL of distilled water and kept for 1 h before filtration on a Büchner funnel. The crude α-cellulose residue was successively washed with 100 mL of 8.3% NaOH solution, 100 mL of distilled water, 15 mL of 10% acetic acid solution and, finally, 250 mL of distilled water. The residual α-cellulose was dried at 103 °C to a constant weight (M<sub>αcellulose</sub>, in mg). α-cellulose content was calculated according to the Eq. (3).

$$\alpha cellulose(\%) = \left[ \frac{M_{\alpha cellulose}}{500 \times (1 + Ext_{tot}\%)} \right] \times 100 \quad (3)$$

The hemicellulose content was then calculated following Eq. (4).

$$Hemicelluloses(\%) = Holocellulose(\%) - \alpha cellulose(\%) \quad (4)$$

#### Klason Lignin Content

Klason lignin content was determined by first mixing 500 mg of sawdust with 72% H<sub>2</sub>SO<sub>4</sub> [Sigma-Aldrich 30743] (10 mL) for 4 h at room temperature. The mixture was then diluted with 240 mL of distilled water, heated under reflux for 4 h and filtered. The residue of Klason lignin thus obtained was washed with hot water and dried at 103 °C to a constant weight (M<sub>KL</sub>, in mg). Klason lignin content was determined by the following Eq. (5).

$$\text{Klason Lignin(\%)} = \left[ \frac{M_{KL}}{500 \times (1 + \text{Ext}_{\text{tot}}\%)} \right] \times 100 \quad (5)$$

### Mineral Composition

Microscopic analysis of the non-sputtered hemp biomass dried for 24 h at 70 °C was performed with a JEOL Scanning Electron Microscope (SEM) IT500 under low vacuum conditions along with Energy-dispersive X-ray Spectroscopy (EDXS) [Oxford Instruments, Link Pentafet] for semi-quantitative determination of its elemental composition.

### Hemp Biochar Particles Preparations

After harvesting, the hemp stalks (with a diameter around 1 cm) were dried at 103 °C for 72 h prior to undergoing a carbonization process. The hemp biochar was produced by pyrolysis of the dry hemp stalks via a Nabertherm RSRC 120-1000/13 tube furnace under an inert N<sub>2</sub> atmosphere (the initial dry weight was measured between 52 and 58 g depending on the batch). Four pyrolysis temperatures (400 °C, 600 °C, 800 °C and 1000 °C) were followed, and the influence of heating rate (200 °C h<sup>-1</sup> and 2000 °C h<sup>-1</sup>) and pyrolysis duration (30 min and 60 min) were studied. After the carbonization process, the samples were removed from the furnace after they cooled below 100 °C. In the study, the samples are references as follows: P[pyrolysis temperature]R [heating rate]T[pyrolysis duration]. Each sample of hemp biochar stalk was then ball milled with water medium in a MillMix 20 homogenizer. Zirconium oxide milling bowls and balls (diameter of 15 mm) were used at 30 Hz frequency for 5 min. The water was then evaporated at 103 °C until a constant mass was reached. For each reference, the final average diameter of the particles for 90% of the distribution (Dv90) was below 90 µm.

### Hemp Biomass and Biochar Analysis

For the proximate and elemental analyses and the calorific values, the raw hemp biomass and hemp biochar samples were ground until reaching a particle size smaller than 0.5 mm and to 100 µm, respectively, and were placed at room conditions.

### Thermogravimetric Analysis of the Hemp Biomass

Thermogravimetric analysis was performed with a LECO TGA801 Thermogravimetric Analyzer with N<sub>2</sub> (10 L min<sup>-1</sup>) as the carrier gas to provide an inert atmosphere for pyrolysis with the same characteristics (heating rate, temperature and duration) as the processing routes described for the

production of biochar in the “[Hemp biochar particles preparations](#)” section. The analysis was done directly on hemp stalks cut at 2 cm (sample weight around 0.5 g) to represent as much as possible the carbonization conditions occurring in the tube furnace and to identify the kinetics of degradation involved for the different processing routes.

### Moisture, Volatile and Ash Content Determination (Proximate Analysis)

The moisture content (MC), volatile matter (VM) and ash contents were determined based on the methodology described in the EN 1860-2 standard for the biochar, and based on the NF EN ISO 18134-3, NF EN ISO 18123 and NF EN ISO 18122 standards respectively for the hemp biomass. For the three determinations, the standards recommend using 1.0 g of material. However, lower amounts were used in this study due to material availability.

For the MC, 1.0 g of raw hemp or hemp biochar sample was heated in the oven at 105 °C until obtention of a constant mass. Then samples were cooled in a desiccator and their mass was measured and compared to their initial mass before heating to determine the MC.

For the VM, approximately 0.5 g of the oven-dried mass ( $M_{\text{oven-dried}}$ ) of each sample was heated in an electric furnace for 7 min at 900 °C without oxygen. Then samples were cooled in a desiccator and their mass was measured ( $M_{\text{Residue}}$ ). The VM was calculated on a dry mass basis according to the Eq. (6).

$$\text{VM(\%)} = \left[ 100 \times \frac{M_{\text{Oven-dried}} - M_{\text{Residue}}}{M_{\text{Oven-dried}}} - \text{MC} \right] \times \frac{100}{100 - \text{MC}} \quad (6)$$

For the ash content, 0.5 g of the oven-dried mass ( $M_{\text{oven-dried}}$ ) of each sample was heated in an electric furnace with air. For raw hemp samples, the temperature was successively increased from ambient to 250 °C in 50 min, maintained at 250 °C for 60 min, then increased from 250 to 550 °C in 60 min and was maintained at 550 °C for 2 h until obtention of a constant mass. For biochar samples, the temperature was successively increased from ambient to 250 °C in 30 min, from 250 to 500 °C in 30 min, from 500 °C to (710 ± 10) °C in 60 min, and was maintained at 710 °C for 2 h until obtention of a constant mass. Then samples were cooled in a desiccator and their mass was measured ( $M_{\text{ash}}$ ). The ash content was calculated on a dry mass basis according to the Eq. (7).

$$\text{Ash content(\%)} = \left[ 100 \times \frac{M_{\text{Ash}}}{M_{\text{Oven-dried}}} \right] \times \frac{100}{100 - \text{MC}} \quad (7)$$

## Fixed Carbon Determination

The fixed carbon (FC) is the carbon remaining after elimination of volatiles and ashes, calculated with the Eq. (8)

$$FC(\%) = 100 - (\text{Volatile content}(\%) + \text{Ash content}(\%)) \quad (8)$$

## Elemental Analysis

Elemental analyses were carried out with an Elemental Vario Macro tube CHN analyzer according to the EN ISO 16948 standard for the raw hemp biomass and ASTM D 5373 standard for biochar samples. Prior to analysis, the samples were packed in tin foil and two tests were performed for each sample. Carbon, hydrogen and nitrogen contents were respectively determined using the quantification of CO<sub>2</sub>, H<sub>2</sub>O and N<sub>2</sub> (after reduction of NO<sub>x</sub>) produced by the combustion of the samples. Oxygen content was calculated by difference, considering the ash content (%), as specified in the Eq. (9).

$$w(O)_d = 100 - w(H)_d - w(C)_d - w(N)_d - \text{Ash content}(\%) \quad (9)$$

With w(O)<sub>d</sub>, w(H)<sub>d</sub>, w(C)<sub>d</sub> and w(N)<sub>d</sub> are, respectively, the oxygen, hydrogen, carbon and nitrogen contents in % by mass of the moisture-free (dry) samples.

$$LHV_{mf}(MJ\ kg^{-1}) = HHV_{mf} - 0.212 \times w(H)_d - 0.0008 \times (w(O)_d + w(N)_d) \quad (14)$$

Atomic H/C and O/C ratios of hemp and its biochar were determined with following Eqs. (10) and (11) [25].

$$\text{Atomic } \frac{H}{C} \text{ ratio} = \frac{\text{Number of H atoms}}{\text{Number of C atoms}} = \frac{\%H/1}{\%C/12} \quad (10)$$

$$\text{Atomic } \frac{O}{C} \text{ ratio} = \frac{\text{Number of O atoms}}{\text{Number of C atoms}} = \frac{\%O/16}{\%C/12} \quad (11)$$

Elemental analyses were duplicated for each sample modality and all the results are given with an accuracy of  $\pm 0.20\%$ .

## Calorific Values

The calorific value was carried out according to the EN ISO 18125 standard, using an Automated Isoperibol Fixed Bomb Parr 6200 bomb calorimeter, under an O<sub>2</sub> atmosphere to ensure the complete sample combustion. Calorimetric Equivalent ( $E_{cal}$ ) was determined before starting experiments using benzoic acid. Approximately 0.5 g mass

of biochar was required to perform the calorific tests. Two replicates minimum were analysed for each biochar material. The higher heating value (HHV) is defined as the amount of heat released by the unit mass of fuel (initially at 25 °C) once combusted and returned to a temperature of 25 °C [12]. The Calorimeter automatically calculates the higher heating value of the as-received sample  $HHV_{ar}$ , taking into account the correction of fuse combustion according to the Eq. (12).

$$HHV_{ar}(MJ\ kg^{-1}) = \frac{K_1 \times E_{cal} \times (T_m - T_i) - K_1 \times L \times E_{pt}}{M} \quad (12)$$

With  $K_1$  a conversion factor ( $4.1855 \times 10^{-6}$  MJ cal<sup>-1</sup>);  $E_{cal}$  the calorimetric equivalent of the calorimeter apparatus in Cal. °C<sup>-1</sup>;  $T_m$  and  $T_i$  are the maximal and initial temperatures in °C;  $L$  is the length of the burnt platinum fuse in cm;  $E_{pt}$  is the platinum's higher heating value at constant volume in cal cm<sup>-1</sup> ( $= 2.3$  cal cm<sup>-1</sup>) and  $M$  is the mass of the sample in kg.

The higher heating value in moisture-free (dry) basis ( $HHV_{mf}$ ) and corresponding lower heating values at constant pressure for a moisture-free (dry) sample ( $LHV_{mf}$ ) were calculated in accordance with CEN/TS 14918 [26] with the Eqs. (13) and (14).

$$HHV_{mf}(MJ\ kg^{-1}) = HHV_{ar} \times \frac{100}{100 - MC} \quad (13)$$

With MC the moisture content of the samples in %, w(O)<sub>d</sub>, w(H)<sub>d</sub> and w(N)<sub>d</sub> are, respectively, the oxygen, hydrogen and nitrogen contents in % by mass of the moisture-free (dry) samples determined in the elemental composition analysis.

Calorific power analyses were duplicated for each sample modality and all the results are given with an accuracy of  $\pm 5.00\%$ .

After carbonization, energy-rich components remain in the biomass, but some energy-lean components are lost. Hence, there is a loss in the overall energy content of the biomass, though there is an increase in the energy density. Energy yield defines this retention, by giving the fraction of the original energy in the biomass retained after carbonization. The energy yield is defined by the Eq. (15).

$$\text{Energy yield}(\%) = \text{Solid yield} \times \frac{HHV_{mf\ biochar}}{HHV_{mf\ biomass}} \quad (15)$$



## Electrical Conductivity

The direct current (DC) electrical conductivity of biochar under compression was measured by the four-point method [27] using a device fabricated at InnoRenew CoE. This device consists of a non-electrical conducting and high-thermal conducting polytetrafluoroethylene (PTFE) die, an oxygen-free, high-conductivity copper base support (99.99% copper content) and a copper piston rod. The piston moved downward into the cylinder under an applied force controlled by a universal test machine, Zwick Z050 [ZwickRoell]. Electrical power was provided by a Keithley 2230G-30-1 triple channel DC power supply (Tektronix, Beaverton, OR, USA) set at 5 V and 1 A. Voltage was measured by a Rigol DM3058 digital multimeter (Rigol, Beaverton, OR, USA) and resulting current directly from the Keithley 2230G-30-1. Conductivity was estimated according to the Eqs. (16) and (17), where  $V$  is voltage of the sample (volt),  $I$  is current of the sample (ampere),  $l$  is height of the sample (cm),  $A$  is area of the piston cross-section (cm<sup>2</sup>).

$$R = \frac{V}{I} \quad (16)$$

$$\sigma = \frac{l}{A \times R} \quad (17)$$

Two specimens were tested for each kind of biochar and all the results are reported here. The volume of samples was estimated according to the Eq. (18) where:  $\pi$  is 3.14,  $r$  is 0.64 cm (i.e., the inner radius of the device) and  $l$  varies with the applied pressure. The initial height of the sample lies between 2.0 and 2.5 cm.

$$volume = l \times \pi \times r^2 \quad (18)$$

## Raman Spectroscopy

Raman spectroscopy analyses were performed directly on ground hemp biochar samples with a Horiba Jobin Yvon LabRAM HR800 Raman spectrometer coupled to an Olympus BXFM optical microscope. Raman spectra were recorded using a 785 nm laser excitation line, a  $\times 50$  long-working-distance objective lens and 600-grooves/mm grating. A multi-channel air-cooled charge-coupled device (CCD) detector was used, with integration time of 20 s and

two accumulations. A laser power at the sample surface was in the range from 1.32 to 1.37 mW. Five Raman spectra were collected on each hemp biochar sample. All the Raman spectra were then baseline corrected and normalized using the OPUS 7.0 data-collection software package (Bruker, Germany).

## Gas Adsorption Analysis

Gas adsorption analysis was performed on the raw hemp biomass and its biochar with an Autosorb iQ-XR-AG-AG [Quantachrome Instruments] Gas Sorption Analyzer. The samples were degassed for 12 h at 100 °C (for the raw biomass) and 250 °C (for the biochar) in vacuum prior to be analysed with CO<sub>2</sub> adsorbate gas. The results were fitted with NLDFT model. From this analysis, only the microporosity of the samples can be investigated (pore size below 2 nm), and the associated surface area.

## Results and Discussion

### Chemical Composition of Raw Hemp Biomass

Table 1 describes the content of the main chemical fractions of the raw hemp biomass constituted of the whole stalk (fibres and hurds indistinctively, with fibres representing 29–32% weight mass of the stalk [1]). Polysaccharides represented by 70.22% of holocellulose content ( $\alpha$ -cellulose, 46.09%, and hemicelluloses, 24.12%) were the most abundant components of hemp stalk, followed by lignin (22.81%), total extractive compounds (4.14%) and ash (2.72%) (Table 1). The chemical composition of the studied hemp was in accordance with those found in the literature. Specifically, Gandolfi et al. [28] found that hemp hurds were composed of 44.0% cellulose, 25.0% hemicelluloses, 23.0% lignin, 4% total extractives (including oil, proteins, amino acids, pectin) and 4% ash. Xie et al. [29] found lower values of polymeric composition concerning the hemp woody core, with 37.3% cellulose, 19.8% hemicelluloses and 12.4% lignin. Ji et al. [30] highlighted that each hemp chemical component showed wide ranges of composition: 32.6–57.5% cellulose, 5.1–28.0% hemicellulose, 12.4–29.4% lignin, 1.2–7.6% ash, 3.7–20.0% extractives and others, depending on the cultivars, varieties and harvesting area.

**Table 1** Chemical composition of the raw hemp biomass (stalk containing fibres and shives)

Chemical composition (in %, oven-dried basis)							
Acetone extractives	Tol:Eth extractives	Water extractives	Total extractives	Holo-cellulose	Hemi-celluloses	$\alpha$ -cellulose	Klason lignin
0.37 $\pm$ 0.04	0.89 $\pm$ 0.07	2.88 $\pm$ 0.03	4.14 $\pm$ 0.14	70.22 $\pm$ 0.56	24.12 $\pm$ 2.31	46.09 $\pm$ 2.73	22.81 $\pm$ 0.14

The successive extraction processes showed that the acetone, toluene:ethanol and hot-water extractive contents were 0.37%, 0.89% and 2.88% (dry basis, from the starting raw material), respectively, reaching a total extractive content of 4.14%. Gutiérrez et al. [31] report the compounds that can be found in the extractives from *Carmagnola* hemp hurds: acetone-CH<sub>2</sub>Cl<sub>2</sub> extractives (1.7% of the starting material) are mainly composed of lipids, which consist mainly of fatty acids, alkanes, aldehydes and sterols; among them phenols, clionasterol, phytosterol and coumarin phenolic compounds

and hot-water extracts (1.6% of the starting material) show the presence of proteins, free amino acids and pectin [31]. Toluene:ethanol extract from hemp hurds (3.5% from the starting raw material) were found to contain mainly extractable waxes, fats and resins [32].

Among the three biomass components, lignin is the most stable, and Burhenne et al. [33] identified it as a key component of the thermochemical decomposition process. These authors observed a slower thermochemical decomposition when lignin content is increased, and the amount of

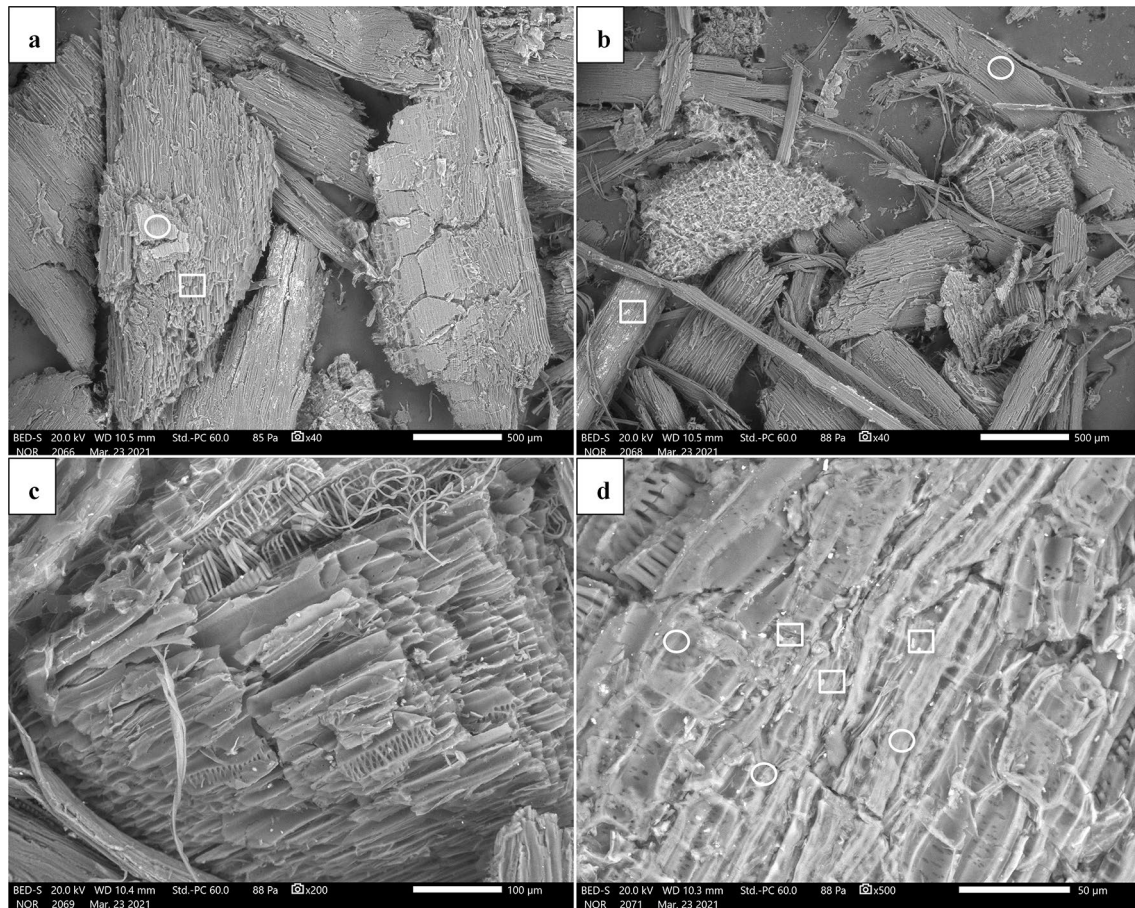


**Fig. 1** SEM micrographs of dry non-sputtered hemp **a**, **b** 40-times magnified, **c** 200-times magnified and **d** 500-times magnified. On marked areas, EDXS was performed; circle marks are mostly organic

material, square marks are material consisting of elements with a higher atomic number than carbon

**Table 2** Average elemental and mineral compositions of the raw hemp biomass according to EDXS analysis performed on the marked areas in Fig. 1

Element	O	C	Ca	K	Al	Cl
White spots (min–max) <i>White square</i>	64.9–71.3	22.5–26.4	0.5–11.8	0.5–0.7	0.04–1.5	0.06–0.3
Grey areas (min–max) <i>White circle</i>	71.0–72.4	26.2–27.1	0.1–1.3	0.2–1.6	0.05–0.06	0.05–0.2
Element	Mg	S	P	Si	Fe	Na
White spots (min–max) <i>White square</i>	0.1–0.9	0.04–0.08	0.06–0.5	1.4*	2.0*	1.1*
Grey areas (min–max) <i>White circle</i>	0.1–0.2	0.04–0.09	0.03–0.1	0.02*	–	0.06*

\*Only one detection of the element

gas product was reduced [33]. Demirbas et al. [34] found a positive correlation between the increase of lignin content in lignocellulosic fuels and their HHV. As a comparison, the lignin content of studied hemp stalk is similar to those of other lignocellulosic biomasses used in energy conversion by torrefaction or carbonization, such as wheat straw (45.20% hemicelluloses, 33.82% cellulose and 20.98% lignin), waste materials (31.42% hemicelluloses, 44.21% cellulose and 24.37% lignin), beech wood (31.86% hemicelluloses, 46.27% cellulose and 21.87% lignin) and hardwood (32.26% hemicelluloses, 45.85% cellulose and 21.89% lignin) [34]. Hemp then appears as a promising candidate for thermal conversion.

Figure 1 shows SEM micrographs of dry non-sputtered hemp stalk biomass. EDXS was performed and elements in marked areas were quantitatively analyzed. While white

circles mark mostly organic material in grey areas, white squares mark white spots where material consists of elements with a higher atomic number than carbon. Table 2 reports the average elemental composition of the raw hemp biomass in the two distinct marked areas. Besides carbon and oxygen that were expected as main elements in cellulose, hemicellulose and lignin, other elements (Ca, K, Al, Cl, Mg, S, P, Si, Fe, Na) were detected in various concentrations. The presence of these elements is explained by hemp plants absorbing both macronutrients (N, K, Ca, P, Mg, S) and micronutrients (Mn, Cu, Zn, Mo, B, Na, Co Fe, Ni, Al) during growth in different concentrations, depending on the plant organ that is considered (leaves, bark or core) and cultivar type [35]. Since the EDXS detects elements from a certain volume, i.e., also below the surface (up to 10  $\mu\text{m}$ ), a portion of the elements identified in the

**Fig. 2** Pyrolysis curves with various heating routes of hemp stalks in TGA

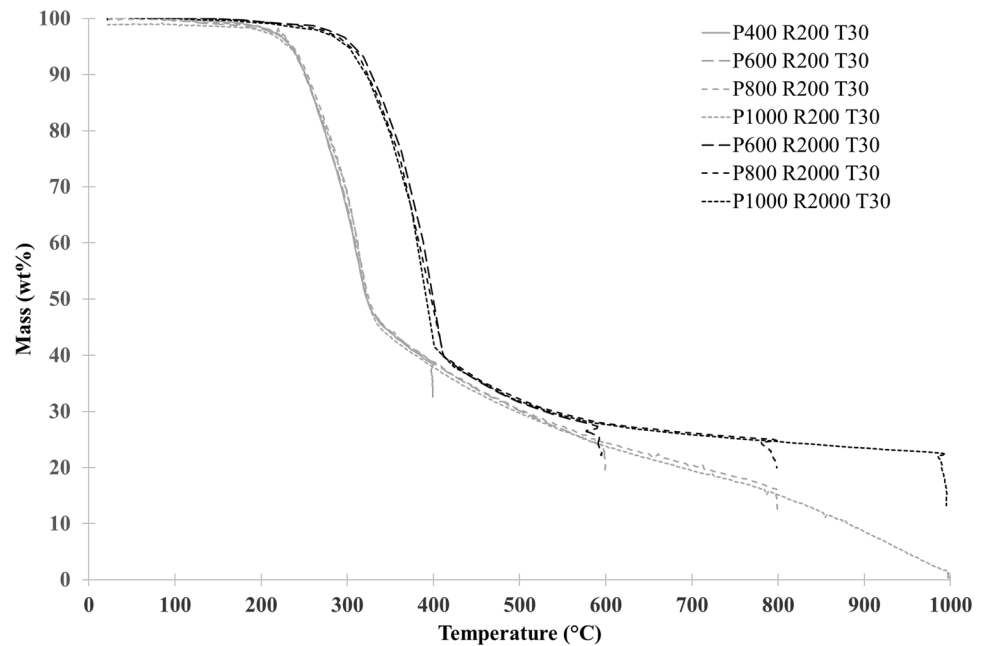


**Table 3** Thermochemical characteristics of hemp stalks in each step for the different processing routes

Sample reference	Stage II			Stage III			End
	$T_{\max}$ (°C)	$DTG_{\max}$ (% °C <sup>-1</sup> )	WL (%)	$T_{\max}$ (°C)	$DTG_{\max}$ (% °C <sup>-1</sup> )	WL (%)	WL (%)
P400-R200-T30	262	0.48	15.29	313	0.75	43.33	66.97
P600-R200-T30	266	0.46	16.83	314	0.87	44.25	79.58
P800-R200-T30	258	0.47	11.65	313	1.03	41.48	89.17
P1000-R200-T30	258	0.44	13.28	316	0.87	44.69	99.68
P600-R2000-T30	335	0.35	14.06	406	0.93	59.78	78.70
P800-R2000-T30	339	0.36	16.14	396	0.76	52.24	80.56
P1000-R2000-T30	337	0.35	17.71	394	0.96	57.54	88.27
P600-R2000-T60	335	0.33	13.70	390	0.81	46.80	81.34
P800-R2000-T60	339	0.36	15.92	393	0.79	50.21	85.51
P1000-R2000-T60	338	0.34	15.98	403	0.81	56.90	93.71



white spots can be attributed to the organic compound below them, and vice-versa for the grey areas.

### Thermogravimetric Analysis of Hemp Stalk During Thermochemical Conversion

The thermograms of the hemp stalk undergoing the different carbonization processing routes are presented in Fig. 2 and the thermochemical characteristics are reported in Table 3. For better visibility, the thermograms of samples that underwent carbonization with 60 min of pyrolysis temperature were not drawn. Biomass pyrolysis results in a series of complex reactions, where components degrade quasi independently, the composition of biomass having predominant influence compared to the interactions among the components [36].

When the temperature increases, a successive decrease of moisture content, hemicellulose and cellulose occurs, after which lignin is decomposed slowly to a minor extent [36]. Prior to undergoing carbonization, moisture was removed from the hemp stalks by drying them for 72 h at 103 °C (Stage I). The mass loss corresponding to the first mass loss observed in Fig. 2 can be attributed mainly to the superposition of the decomposition of hemicellulose that occurs between 220 and 315 °C, and the decomposition of cellulose between 315 and 400 °C [37]. The maximum mass loss rate (Table 3) associated with the decomposition of hemicellulose (Stage II) was recorded between 258 and 266 °C for the lower heating rate (200 °C h<sup>-1</sup>) and between 335 and 339 °C for the higher heating rate (2000 °C h<sup>-1</sup>). Similarly, the maximum mass loss rate associated with the decomposition of cellulose (Stage III) was recorded between 313 and

316 °C for the lower heating rate (200 °C h<sup>-1</sup>) and between 390 and 406 °C for the higher heating rate (2000 °C h<sup>-1</sup>). The decomposition of hemicellulose and cellulose was then shifted to higher temperatures when the heating rate was increased. This shift might be due to the heating through the surface happening in the tube furnace (as opposed to a volumetric heating which would occur with microwaves). Hence more time is needed for the material to fully heat onto the chosen temperature, and for the chemical reactions to take place. Similar thermal degradation kinetic tendency was observed during the pyrolysis of pure cellulose, hemicellulose and lignin fraction [38]. Moreover, the degradation kinetics and weight losses for Stage II and Stage III are different depending on the heating rate (Table 3). The heating rate then influenced the type of degradation products. During Stage II, weight loss varied between 11.65% and 17.71%. The hemicellulose content of the raw hemp biomass was found to be 24.12% in the previous section, indicating that some hemicellulose residues are still present at the end of Stage II. Yang et al. [37] found about 20% solid residue of hemicellulose at 900 °C, which is in accordance with the highest hemicellulose weight loss of this study. During Stage III, weight loss varied from 41.48 to 59.78%. Knowing that the  $\alpha$ -cellulose content was found to be 46.09%, and that Yang et al. [42] observed a low residual cellulose residue of 6.5% at 900 °C, the weight loss observed during Stage III probably included subsequent degradation of hemicelluloses and lignin besides cellulose. The decomposition of lignin was not evident from the observation of the curves since it was spread on a large temperature range (from 160 to 900 °C [37]) with a low mass-loss rate. The final mass residue decreased when the carbonization temperature

**Table 4** Composition of the hemp biomass and its biochar

Sample reference	Proximate analysis (wt %)*				Elemental analysis (%)**					
	FC	Moisture	Ash	VM	C	H	N	O	H/C	O/C
Hemp biomass	25.2	6.76	2.7	72.1	45.6	6.2	0.3	45.2	1.63	0.74
P400-R200-T30	66.1	2.50	6.8	27.1	73.8	3.8	0.6	14.9	0.61	0.15
P600-R200-T30	82.6	2.25	6.5	10.9	86.8	2.0	0.8	3.7	0.27	0.03
P800-R200-T30	85.5	2.02	6.7	7.8	89.1	0.7	0.9	2.5	0.10	0.02
P1000-R200-T30	85.7	2.26	8.9	5.5	87.3	0.3	1.3	2.0	0.05	0.02
P600-R2000-T30	78.8	1.89	9.8	11.6	83.8	1.8	0.7	3.9	0.26	0.03
P800-R2000-T30	83.8	2.38	8.4	7.9	87.5	0.6	0.9	2.2	0.08	0.02
P1000-R2000-T30	81.9	2.27	10.3	7.9	87.8	0.2	1.1	0.1	0.03	0.00
P600-R2000-T60	79.8	2.08	9.7	10.4	84.5	1.8	0.8	2.9	0.26	0.03
P800-R2000-T60	84.7	1.65	7.7	7.6	87.9	0.9	1.1	2.2	0.12	0.02
P1000-R2000-T60	79.6	2.30	11.3	9.1	86.7	0.2	1.1	0.3	0.03	0.00

\*Dry mass basis. FC results are given with an accuracy of  $\pm 0.20\%$ , Moisture contents are given with an accuracy of  $\pm 0.20\%$ , Ash contents are given with an accuracy of  $\pm 5.00\%$  and Volatile contents are given with an accuracy of  $\pm 1.00\%$

\*\*Dry mass basis. Each analysis has been duplicated and all the results are given with an accuracy of  $\pm 0.20\%$

increased, and the higher heating rate led to a lower final weight loss. Additionally, the higher the considered carbonization temperature, the lower the final weight loss (at 600 °C, the weight loss is 1.1% lower for the samples heated at 2000 °C h<sup>-1</sup> vs 200 °C h<sup>-1</sup>, and at 1000 °C, the mass loss is 11.4% lower). Yang et al. [37] report that lignin solid residue after pyrolysis at 900 °C was the highest, around 45.7 wt %. This value is in accordance with the solid residue observed in this study at 800 °C.

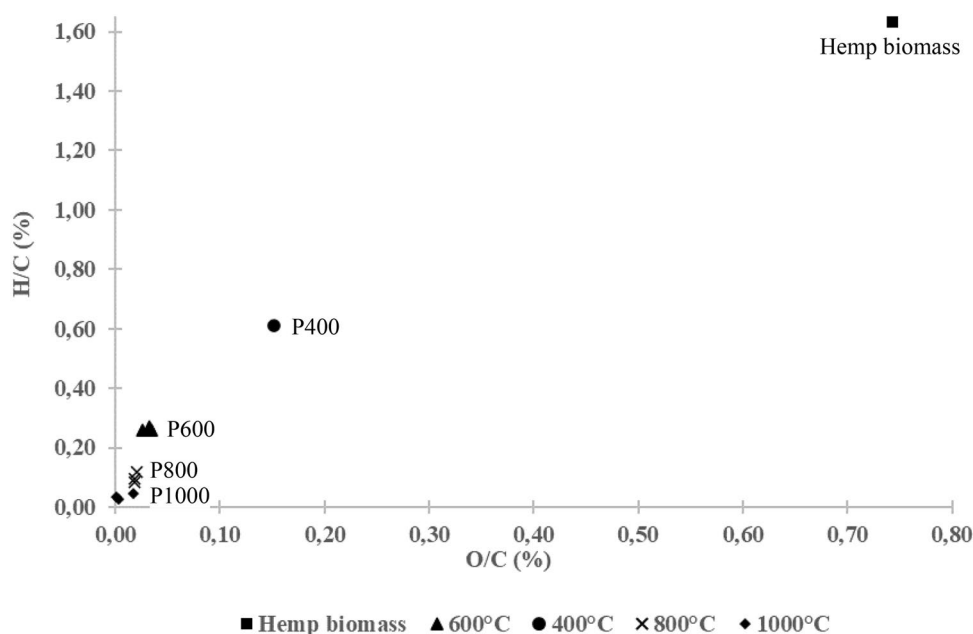
### Evolution of the Elemental Composition Through Carbonization Process

The elemental analysis (Table 4) showed that the hemp biochar had a higher concentration of carbon (C) and lower content of oxygen (O) than the raw feedstock material. The raw hemp is composed of 45.6% carbon, 45.2% oxygen, 6.2% hydrogen and 0.3% nitrogen, on a feedstock-dried basis. Our results are consistent with those issued from the literature, highlighting that C content of raw hemp biomass varies from 45 to 49% [4], O from 39 to 45% [4], H from 5.6 to 6.2% [4], N from 0.3 to 1.3% [4]. The oxygen and hydrogen composition of hemp is similar to other energy crops (cereals, miscanthus, reed canary grass) [4], and the high carbon content suggests a strong energy density. Past literature suggests that the higher the C percentage, the higher the HHV, regardless of the raw lignocellulosic materials [39]. This relationship is considered to occur, as C and H are responsible for the energy content in biofuels, due to exothermal reactions that take place with O<sub>2</sub> during combustion, generating CO<sub>2</sub> and H<sub>2</sub>O, respectively [40]. The carbon content of hemp-derived biochar increased with the increasing carbonization

temperature up to 800 °C. No significant improvement in carbon content was found when carbonizing to 1000 °C. The contents of hydrogen and oxygen decreased continuously from 400 to 1000 °C. Then increasing the carbonization temperature up to 800 °C increased the fuel quality in terms of energy density. The amount of nitrogen (N) in solid biofuel is important because this element can form gaseous nitrogen oxide pollutants NO<sub>x</sub> [13]. The N content in the hemp feedstock material was 0.3% and increased with an increase of the carbonization temperature of the biochar, reaching a maximum of 1.3% for the sample P1000-R200-T30. Askeland et al. [41] showed a similar tendency concerning the nitrogen content increase for pyrolysis of pine wood (N=0.15%), from 350 °C (N=0.25%) to 750 °C (N=0.56%). However, their research indicated that nitrogen was not affected by higher pyrolysis temperature when carbonizing straw. Yousaf et al. [16] observed that the nitrogen content of peanut shells and wheat straw biochar decreased with increasing carbonization temperature (300 °C, 500 °C, 700 °C). In fact, the nature of the feedstock was the main factor affecting nitrogen evolution during the pyrolysis process. Due to the varied biochemical composition of each biomass, even within the same type of biomass, the trends of the N transformation according to pyrolysis severity is not obvious [42]. In general, lipid and protein-rich biomasses produce biochar with low yield, resulting in less retention of N in biochar. On the other hand, carbohydrates such as lignin, cellulose and hemicellulose favor the production of biochar [43]. The higher content of carbohydrates can also promote the retention of more N in biochar [44].

The H/C and O/C atomic ratios are indicators of the degree of aromaticity and carbonization. Hemp feedstock

**Fig. 3** Van Krevelen diagram for hemp biomass and its biochar



biomass presented much higher ratios of H/C and O/C than biochar (Table 4), as reported in the literature [45]. The H/C and O/C ratios of the hemp biochar decreased with increasing carbonization temperature. A higher heating rate tended to decrease the H/C ratio at a given temperature. Variations in H/C and O/C ratios were too low to conclude the influence of the pyrolysis duration on the atomic ratios. The Van Krevelen diagram (H/C vs O/C ratios) was plotted in Fig. 3. The results indicated that both ratios decreased when the temperature increased, and that the biochar carbonized at 1000 °C showed the lowest values for both ratios. Losses in hydrogen and oxygen are linked to the breakage of large hydrocarbon molecules of biomass during the carbonization to form smaller molecules like water, dihydrogen, carbon monoxide and dioxide and other gaseous light hydrocarbon  $C_xH_yO_z$  compounds besides solid carbon. Besides the loss of hydrogen and oxygen in the volatile matter, Shafizadeh et al. [46] suggested that a more aromatic carbon structure of biochar results at higher pyrolysis temperatures, which explains the decrease in the H/C ratio, as observed in this study. These authors [46] reported that the mainly aliphatic carbon structures in the polymer units of cellulose changed after pyrolysis to a mix of aliphatic, alkene, aromatic, carboxylic and carbonyl carbon structures. Wyn et al. [45] associated energy densification in the biochar samples with the loss of compounds containing hydrogen and oxygen during the pyrolysis process.

### Chemical Characterization: Hemp Biomass and Biochar

The proximate compositions—fixed carbon (FC), moisture, ash content (ash), volatile matter (VM)—of the raw hemp biomass and its biochar are presented in Table 4. Moisture content decreased from 6.76% for the hemp feedstock to 1.65–2.50% for the hemp biochar. Water is retained in biomass by hydroxyl and hydrophilic groups. When biomass is decomposed, adsorption sites are reduced and water evaporates [14]. The moisture content hinders the combustion and influences the volume of flue gas produced per energy unit [14]. Thanks to the diminution of moisture content brought by the carbonization process, the quality of biochar as solid biofuels increased compared with initial hemp feedstock.

Native hemp stalks were composed of 25.2% FC, 2.7% ashes and 72.1% VM. Similar proximate compositions were found by Kraszkiewicz et al. [47] and Wallace et al. [48] who highlighted that *Cannabis sativa* hurds have VM and FC around 69.66% and 18.8%, respectively, and ash contents varied from 0.9 to 2.51%. Other literature reports more scattered values as FC (8.9–10.3%wt) [49], VM (87.5–87.9%wt) [49], ash (2.2–3.2%wt) [49], showing that the proximate composition of raw hemp greatly varies depending on the species [35] and the growing area and processing (retting

and decortication) of the plant [49]. We observed a clear augmentation of the FC content (from 66.1 to 85.5%) when the temperature was increased from 400 to 800 °C, with no significant change with further increased temperature. The higher heating rate led to a relatively small decrease in the FC. Increasing the carbonization duration from 30 to 60 min did not have a significant effect on the FC. The VM of a fuel is the condensable and non-condensable vapor released when the fuel is heated. The removal of VM during pyrolysis pretreatment produces biochar that is expected to show lower particle matter emissions. Indeed, recent studies demonstrated that carbonized biomass emits less particle matter compared with raw biomass [7, 50]. As highlighted by TGA, the types of degradation products differ with the heating rate, which explains the observed differences in VM. For the samples treated with a heating rate of 200 °C min<sup>-1</sup> for 30 min, VM decreases according to the temperature level increase (from VM = 27.1% for the P400-R200-T30 sample to VM = 5.5% for the P1000-R200-T30 sample). At mild temperature (600–800 °C), the increase of heating rate undergoes a decrease of VM. On the other hand, samples heat-treated at 1000 °C present an increase in VM according to the increase of heating rate. Similar tendencies are observed concerning the impact of the pyrolysis duration. At 600 °C, a prolonged pyrolysis duration tended to slightly decrease the VM, leaving more time for the degradation of components to happen and escape as gaseous reaction products. According to the literature, the longer the residence time, the higher the carbon content as larger quantities of volatile matter are being released [55]. However, for the samples treated at 800 °C and 1000 °C, with a heating rate of 2000 °C min<sup>-1</sup>, a prolonged pyrolysis duration tended to increase the VM. According to the literature, rapid pyrolysis (high heating rate) results in more VM than a low pyrolysis-heating rate [56]. VM mainly consists in heavy compounds with a high C/H ratio. Mermoud et al. [51] showed that pyrolysis performed with a low temperature and a high heating rate undergoes a rapid increase of pressure into the biomass particle and an explosive release of gases leading to a rapid formation of VM. In contrast, a high pyrolysis temperature coupled with a high heating rate increases the occurrence of polymerization of volatiles within the biochar [56], leading to a low amount of VM produced during thermochemical degradation. These secondary reactions take place upon contact with the biochar and generate lighter compounds with a lower C/H ratio, re-forming charcoal at the surface of the solid. The char yield is then increased compared to rapid pyrolysis. Above 800 °C, the decline in VM was proportionally lower and constant, indicating the formation of the most stable carbonaceous compound in terms of material loss [52]. Other studies have also shown a similar correlation for other materials where a rapid initial decline in yield was present at lower temperatures, followed

by a smaller and constant reduction at higher temperatures [53, 54]. Liu et al. [14] underlined an easier control of the combustion process when using fuel with lower VM content. This result implies for our study that biochar produced at pyrolysis temperature up to 800 °C for both heating rates are the most suitable for solid biofuel application as they had the lowest VM.

The ash content reflects the mineral matter in the samples. The EDXS analysis identified the presence of Ca, K, Al, Cl, Mg, S, P, Si, Fe and Na elements in the raw hemp biomass of this study. The major ash-forming elements are reported to be Ca, K, Mg, Al, Fe, Mn and Na [4]. Either the variety, location or year of culture do not significantly affect their amount in the plant [4]. However, the ash content of hemp biomass is dependent on the harvesting date [4]. Indeed, a decrease in the content of ash-forming elements with a delay of harvest has been reported [4], due to the nutrient losses from the plants' leaves that wither and fall and wash-out effects by precipitation. In this study, the observed ash content for the hemp feedstock (2.7%) is lower than values reported in the literature for summer- or autumn-harvested hemp (6.6–8.6%) [4]. This lower content could be explained by stalk being harvested during the spring season. Past research found that the ash content of hemp was considerably lower during spring than those of hemp harvested during winter or autumn seasons [4]. Concerning hemp biochar, ash contents varied between 6.5 and 11.3%. The ash content increased slightly (in most cases) with increasing carbonization temperature, regardless of the heating rate or carbonization duration. The ash content increase with the increasing carbonization temperature can be explained by the concentration of inorganic minerals and the formation of their oxides and carbonates. Fouling issues during the combustion process can be expected from a high ash content

[8]. This phenomenon should be considered when selecting process parameters for the thermochemical conversion of hemp.

### Energy Properties of Hemp Biomass and Biochar

The higher heating values (HHV) and lower heating values (LHV) of the hemp biomass and biochar are reported in Table 5. HHV reflects the combustibility of solid fuels. Since the moisture slightly varies from one sample to another, the moisture-free values of HHV and LHV are used for the comparison. In this study,  $\text{HHV}_{\text{mf}}$  and  $\text{LHV}_{\text{mf}}$  of hemp raw biomass are  $18.77 \text{ MJ kg}^{-1}$  and  $17.50 \text{ MJ kg}^{-1}$ , respectively. Past research reported values for HHV of hemp ranging from 17.9 to  $19.1 \text{ MJ kg}^{-1}$ , depending on year, location of cultivation and harvesting period [4], which is in accordance with the data of this study. For a given hemp biochar sample,  $\text{HHV}_{\text{mf}}$  and  $\text{LHV}_{\text{mf}}$  values are very close since H, O and N atomic contents are low.  $\text{HHV}_{\text{mf}}$  increased with the carbonization temperature from  $18.77$  to  $28.45 \text{ MJ kg}^{-1}$  and to  $30.95 \text{ MJ kg}^{-1}$  for biochar carbonized at 400 °C and at 600 °C respectively. Yousaf et al. [16] also observed an increased energy content HHV with an increase in pyrolysis temperature and reported maximum HHV values at  $28.79 \pm 0.34 \text{ MJ kg}^{-1}$  and  $24.07 \pm 0.35 \text{ MJ kg}^{-1}$  for peanut shell and wheat straw biochar produced at 700 °C, compared to  $18.10 \pm 0.27 \text{ MJ kg}^{-1}$  and  $15.54 \pm 0.28 \text{ MJ kg}^{-1}$  for their corresponding feedstocks. By performing a pyrolysis process under a temperature of 500 °C, Raveendran and Ganesh [55] showed that HHV of coir pith, corn cob, groundnut shell, rice husk and wood improved from 19.5 to 25.0, from 16.1 to 28.6, from 19.8 to 27.4, from 20.0 to 44.2 and from 20.0 to  $24.1 \text{ MJ kg}^{-1}$ , respectively.

**Table 5** Energy recovery, calorific values, carbon structure (by Raman Spectroscopy) and surface area (SA) (by CO<sub>2</sub> absorption) of the hemp biomass and its biochar

Sample reference	Energy recovery		Calorific values		Carbon structure			Surface SA (m <sup>2</sup> g <sup>-1</sup> )
	Solid yield (%)	Energy yield (%)	$\text{HHV}_{\text{mf}}$ (MJ kg <sup>-1</sup> )	$\text{LHV}_{\text{mf}}$ (MJ kg <sup>-1</sup> )	D-band	G-band	I <sub>D</sub> /I <sub>G</sub>	
Hemp biomass	100	100.00	18.77	17.50	–	–	–	93
P400-R200-T30	41	62.14	28.45	27.64	–	–	–	301
P600-R200-T30	29	31.55	30.95	30.52	1317	1579	1.41	478
P800-R200-T30	34	33.27	30.29	30.14	1306	1583	1.57	726
P1000-R200-T30	36	34.66	29.16	29.10	1298	1593	1.73	444
P600-R2000-T30	28	29.41	30.63	30.24	1312	1584	1.37	517
P800-R2000-T30	28	26.67	29.18	29.05	1307	1590	1.58	756
P1000-R2000-T30	27	25.72	27.80	27.75	1302	1587	1.85	524
P600-R2000-T60	27	29.32	30.19	29.80	1321	1582	1.46	420
P800-R2000-T60	38	36.54	29.03	28.85	1301	1587	1.68	590
P1000-R2000-T60	28	28.06	29.09	29.05	1305	1594	1.75	233



They also analysed the influence of pyrolysis on an isolated fraction of cellulose, lignin and xylan, showing that HHV was improved from 11.7 to 32.4, from 24.1 to 33.3 and 30.4 to 32.3 MJ kg<sup>-1</sup>. Demirbas [56] reported that the HHV of lignin was higher than the ones of cellulose and hemicellulose due to their higher degree of oxidation. Above 800 °C, there was a slight decrease in HHV<sub>mf</sub> and LHV<sub>mf</sub>. This thermal efficiency seemed to slightly decrease for a higher heating rate or a longer pyrolysis duration. To ensure auto-thermal combustion, a solid fuel should have an HHV value higher than 20 MJ kg<sup>-1</sup> [13]. The biochar produced with all the processing routes considered in this study are then able to satisfy this requirement though. The literature reports that low H/C and O/C

ratios correspond to high HHVs [12, 25]. In the study, this correspondence was verified only to a certain extent since biochar carbonized at 1000 °C presented the lowest H/C and O/C ratios, but not the highest HHVs. Similar results have been found by Ronsse et al. [57] performing various pyrolysis processes (temperature ranged from 300 to 750 °C, durations of 10 min and 60 min) on dry algae, green waste, straw and wood. In particular, they showed that for pyrolysis temperature higher than 600 °C, H/C ratios for each sample continue to decrease, whereas HHV tends to be stabilized or slightly decrease. Finally, increasing the pyrolysis temperature from 400 to 600 °C led to the production of denser energy-dense fuel but decreased by 2 times the energy yield (Table 5). From

**Fig. 4** Electrical conductivity behaviour of the biochar powders as a function of the pressure. ○, △ symbols represent hemp biochars carbonized at 1000 and 800 °C respectively. Empty and plain symbols are used for carbonization carried out at 200 °C h<sup>-1</sup> and 2000 °C h<sup>-1</sup> respectively. Black and grey filling are used for residence time for 30 and 60 min respectively

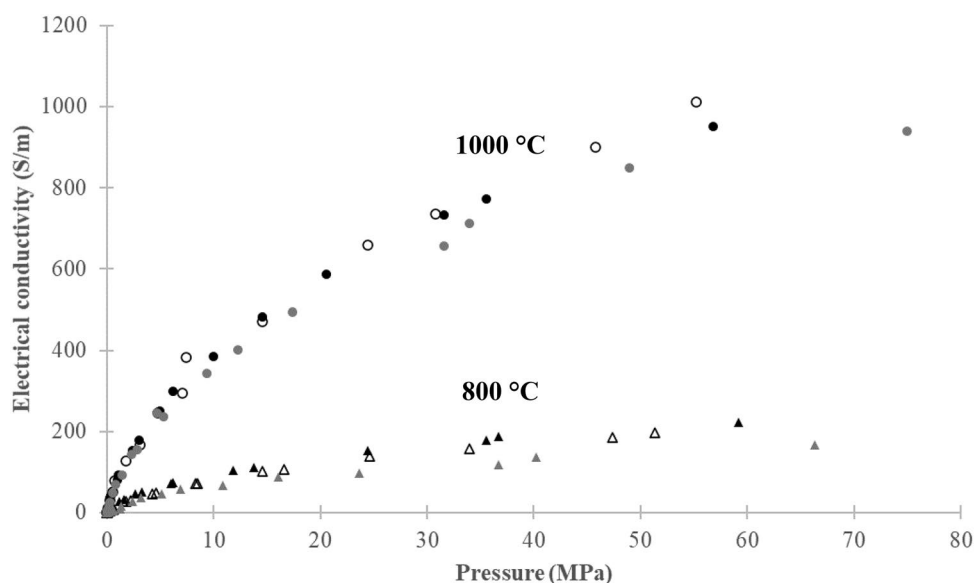
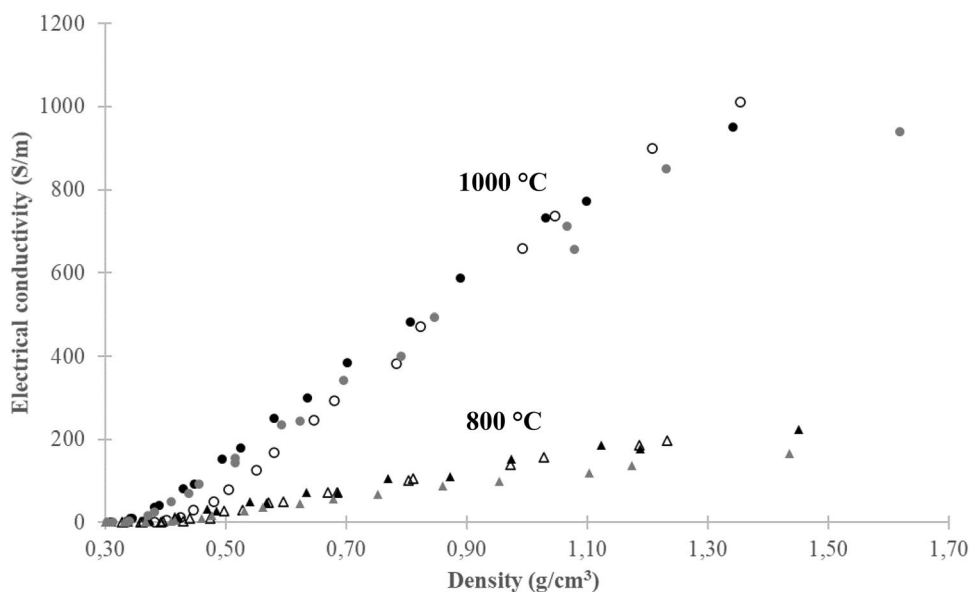


**Fig. 5** Electrical conductivity behaviour of the biochar powders as a function of the density. ○, △ symbols represent hemp biochars carbonized at 1000 and 800 °C respectively. Empty and plain symbols are used for carbonization carried out at 200 °C h<sup>-1</sup> and 2000 °C h<sup>-1</sup> respectively. Black and grey filling are used for residence time for 30 and 60 min respectively



600 °C and above, the energy yield was close to 30%, whatever the heating rate or residence time. These findings allow classifying hemp biochar (400–600 °C) among the lignocellulosic materials with a good potential toward energy conversion.

### Electrical Properties of Hemp Biochar

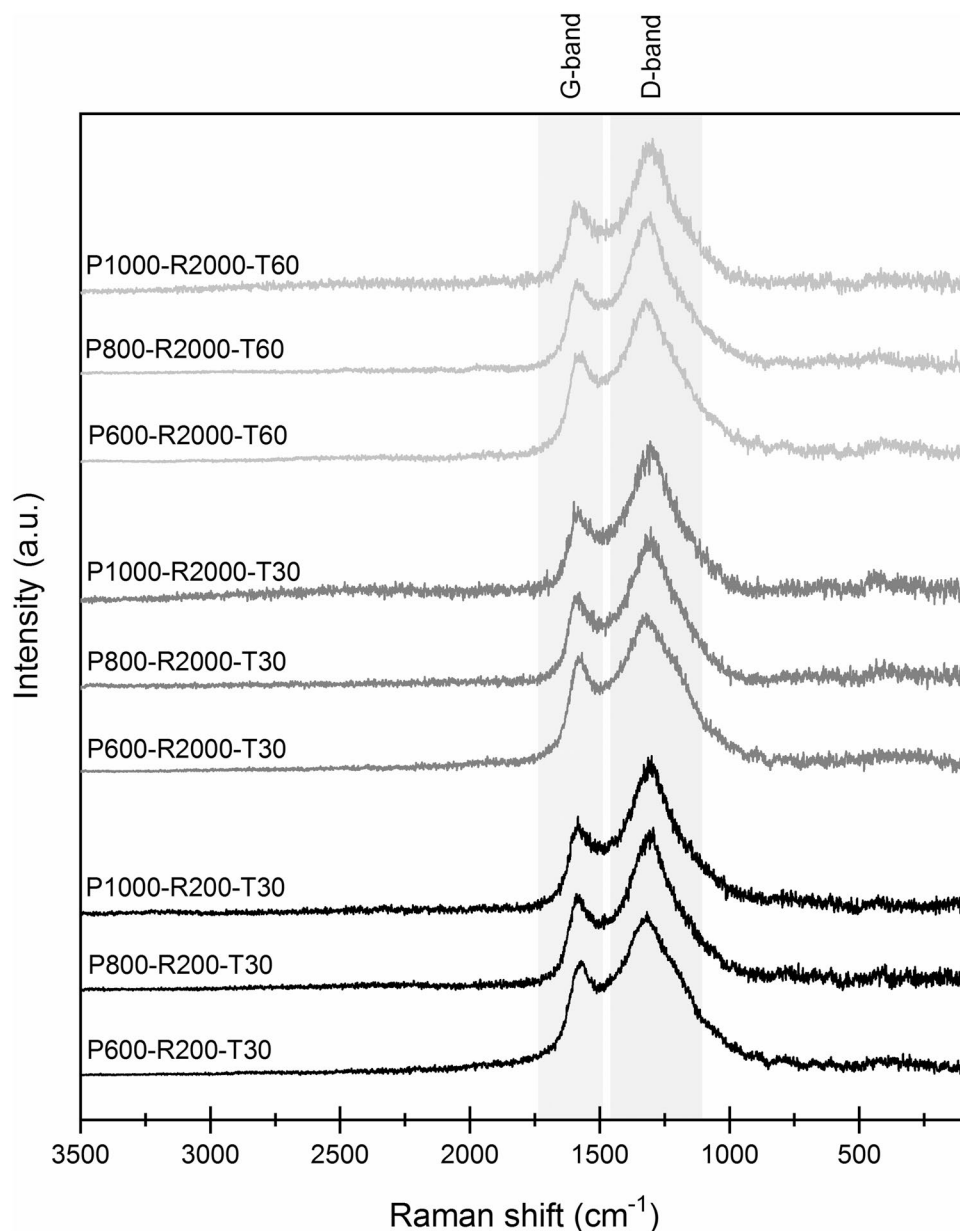
The electrical conductivity of the biochar was measured under compression. The results are plotted versus pressure applied on the biochar particles (Fig. 4) and versus density of the compacted biochar particles (Fig. 5). The plots for the biochar produced at 400 °C were not displayed as these samples did not have any measurable electrical conductivity at any compaction density. The hemp biochar produced at 600 °C displayed a weak electrical conductivity ( $0.01 \text{ S m}^{-1}$ ) for the best cases at pressures higher than 5 MPa and associated density higher than  $0.6 \text{ g cm}^{-3}$ , and therefore is not drawn on the figure for clarity. The results of the conductivity tests indicated that higher pyrolysis temperatures resulted in higher biochar electrical conductivity for a given pressure or density. Shao et al. [58] similarly began to measure DC electrical conductivity of chars sheets from microfibrillated cellulose/lignosulfonate precursors for carbonization temperatures higher than 600 °C, and observed a linear increase of conductivity between 700 and 1000 °C. The electrical conductivity of the hemp biochar at a given temperature increased with the applied pressure and density, as the contact between particles increased and the inter-particle resistance to the electrical charge transport decreased. Moreover, the variation in conductivity decreased with the increase of pressure. The hemp biochar produced at 600, 800 and 1000 °C contained more than 83.8% of carbon (measured by elemental analysis, see Table 4). However, the electrical conductivity cannot be only related to the carbon content since this one was stable or decreased above 800 °C while the conductivity was clearly superior for biochar carbonized at 1000 °C.

The CO<sub>2</sub> gas adsorption analysis gave access to the surface area associated to the microporosity (pore size below 2 nm) of the raw hemp biomass and its biochar (Table 5). For a given heating rate ( $200 \text{ °C h}^{-1}$  or  $2000 \text{ °C h}^{-1}$ ), the surface area associated to microporosities substantially increased with increasing carbonization temperature up to 800 °C, and drastically decreased at 1000 °C (Table 5). For the same carbonization temperature, the microporosity was higher for the higher heating rate. This microporosity is believed to be due to the evacuation of volatile matter (VM) during the thermochemical process. Indeed, measured surface area concurrently increased with the amount of evacuated VM. At a given heating rate ( $2000 \text{ °C}$ ), when residence time was increased from 30 to 60 min, the microporosity decreased for a given temperature, with the magnitude of the

drop increasing with increasing temperature (ratio of microporosities after 30 and 60 min was 1.23 for 600 °C, 1.28 for 800 °C and 2.25 for 1000 °C). These observations translate a rearrangement of the biochar microstructure along with an extended duration of the thermochemical conversion.

The Raman spectroscopy was used to evaluate the development of graphite like microstructures, since this technique is highly sensitive to sp<sup>2</sup> carbon structures [59, 60]. The Raman spectra of the biochar carbonized at 400 °C did not display any identifiable peak (Raman spectrum not shown). For all biochars carbonized at 600 °C and above temperatures, two main peaks were identified in the Raman spectra placed at  $1579\text{--}1594 \text{ cm}^{-1}$  (G band) and  $1298\text{--}1321 \text{ cm}^{-1}$  (D band) (see Fig. 6). The presence of the 2D band (between  $2500$  to  $2900 \text{ cm}^{-1}$ ) related to the interaction of stacked graphene layers is not visible. Escribano et al. [61] reported that a strong and narrow 2D band in the spectra is representative of an ordered carbon material, while has a weak and broad 2D band characterized a carbon material with extensive disorder or very small crystal size. In our case, the absence of 2D band combined with the presence of distinct G and D bands suggested an intermediate structure between ordered and disordered crystals. The structure of activated carbon was similarly described as intermediate with a lack of 2D peak but fairly narrow D and G peaks [61]. The G band is related to the sp<sup>2</sup> bonded carbon structures [61] and rises in highly ordered carbon structures such as graphite, whereas the D band is related to the disorder around sp<sup>2</sup> carbon, such as defects, distortions and edges in the crystal structure [62]. Even if the D band is associated with the extent of defects, this band appears in the presence of ordered carbon structures (aromatics with more than 6 fused benzene rings [63]). The elemental analysis suggested that biochar produced at higher pyrolysis temperatures had a more aromatic carbon structure, highlighted by the decrease in the H/C ratio. The H/C ratio dropped from 0.61 for the biochar produced at 400 °C, to 0.26–0.27 for the biochar produced at 600 °C, where the D-band started to be visible. The ratio between the intensity of the D band and the G band ( $I_D/I_G$ ) (Table 5) was used to compare the structure ordering of the hemp biochar, as commonly described in the literature for studying the highly ordered carbon materials [60, 64]. However, care should be taken when interpreting the Raman spectral data for these highly disordered “non-graphitizable” carbons [59] and the  $I_D/I_G$  ratio cannot be directly compared to the results that can be obtained for highly ordered carbon materials [63]. Our results (Table 5) indicated a clear increase of the  $I_D/I_G$  ratio with the increase of the carbonization temperature, with no significant influence of the chosen heating rate or residence time on the ratio. Such an increase ( $I_D/I_G$  from 2.6 to 3.8) was previously reported [58] for microfibrillated cellulose/lignosulfonate biochar produced from 400 to 1000 °C, with a stabilization of the ratio for temperatures

**Fig. 6** Raman spectra of carbonized biochar samples. The light greys rectangles indicate the characteristic G and D bands of hemp biochar



above 1000 °C. Other authors [59, 63] report an increase of the  $I_D/I_G$  ratio for biochar from various biomasses (Victorian brown coal, sucrose, harakeke, radiata pine wood) carbonized from 400 to 1000 °C. This increase was attributed to the rise of defects or growth of edge bonded graphite-like structures, revealing a bigger concentration and/or size of aromatic clusters towards graphene-like networks [59, 63]. Moreover, the hemp biomass precursor is rich in oxygen (45.2% see Table 4), with 0.1 to 2.0% remaining after carbonization at 1000 °C. The presence of oxygen is partly responsible for defects observed in the graphite-like structure. Indeed, it has been shown [65] that introduction of oxygen through high pressure oxidation changed an easily graphitizable carbon material to a non-graphitizable one.

The G band position was found to blueshift toward higher frequencies when the carbonization temperature increased, whereas the D band tended to move towards lower positions (see Table 5). The G band position is reported to be strain-related [66]. During the thermochemical treatment, aromatic clusters become larger and their graphite-like structure increase, so they enter in collision, get more compressed and eventually merge with surrounding clusters within a limited volume [59]. The G band blueshift might then indicate the growth of ordered carbon clusters. Similarly, the redshifting D band position can be interpreted as reflecting the increasing tensile strain related to the near-edge structures [66] and provides information about the most common types of near edge structures that can be found around the ordered carbons

[59]. Hence, the D band position of the biochar produced at 600 °C (1312–1321  $\text{cm}^{-1}$ ) is close to the D band position of synthetic graphite (around 1316  $\text{cm}^{-1}$ ) [59], suggesting that the edges become similar to those occurring in graphite. With a temperature increasing to 800–1000 °C, the D band position moves to 1298–1307  $\text{cm}^{-1}$ , indicating a fullerene-like more pronounced curvature of the edges (fullerene D band position close to 1300  $\text{cm}^{-1}$  [67]).

The electrical conductivity is strongly related to the microstructure of the hemp biochar, that evolves with the temperature of the thermochemical process. Below 600 °C, amorphous phases predominate in the carbon structure (D and G bands not identified by Raman spectroscopy). Moreover, the microporosity increases due to the evacuation of volatiles, and prevents the electrical charge transport because of the intra-particle resistance. In consequence, the DC conductivity was not detected. Between 600 and 800 °C, the VM stabilized (VM was measured between 7.6 and 11.6%, see Table 4) and the surface area linked to the presence of microporosities was the highest at 800 °C. The amorphous phase decreased (apparition of D and G bands in the Raman spectra), and the defected graphene structures grew and became denser, with increasing  $I_D/I_G$  ratio and observed shifts of D and G bands. The contact between defected graphene structures upon a percolation threshold allowed electron's mobility and the detection of electrical conductivity that increased with the compaction of defected graphene clusters. Between 800 and 1000 °C, graphite-like structures keep growing and packing (increasing  $I_D/I_G$  ratio), intensifying electrical pathways. Simultaneously, the rearrangement of the microstructure was associated to a strong decrease in microporosities, lowering the intra-particles resistance and further increasing the DC conductivity.

## Conclusions

The presented research investigated the thermal, chemical, physical, electrical and energy properties of hemp stalks enhanced through thermochemical conversion for renewable energy applications. Influence of the thermochemical conversion processing parameters such as pyrolysis temperature, heating rates and residence time was studied in regard with the properties of interest related to fuel and energy applications. The chemical composition of the hemp stalks showed lignin content similar to those of other lignocellulosic biomasses used in energy conversion by torrefaction or carbonization, which placed hemp as a promising biomass for the thermochemical conversion. Two ways of valorisation of the hemp biomass were clearly identified, depending mainly on the chosen pyrolysis temperature. Hemp biochar carbonized at 400–600 °C were classified as lignocellulosic materials with a good potential for solid biofuel applications.

Specifically, the resulting carbonized biochar presented low moisture content (high fuel quality), low VM content (so likely to show lower particle matter emissions), limited ash content (low risk of fouling issues during the combustion), high carbon content (suggesting strong energy density) associated with fairly high HHVs and optimized energy yield. Hemp biochar carbonized at 800–1000 °C displayed interesting electrical conductivity, opening opportunities for its use in electrical purposes. The electrical conductivity was related to the evolution of the biochar microstructure (development of graphite-like structure and changes in microporosity) in regard with the thermochemical conversion process parameters. The thermochemical conversion of hemp biomass is believed to present a relatively simple and easy-to-scale-up method to value hemp by-products from CBD industry. Indeed, hemp stalks collected after harvest would not need a specific pre-processing step, besides drying, prior to undergoing carbonization and fit well as a suitable fuel product. Further investigation into additional activation steps is necessary, however, to fully develop the carbonized hemp for some specific electrical applications (e.g., supercapacitor electrodes).

**Author contributions** LM: Methodology, Investigation, Visualization, Writing—Original Draft, Writing—Reviewing and Editing, Funding Acquisition; KC: Investigation, Validation, Writing—Original Draft; JV: Investigation; CL: Investigation; BH: Investigation; LL: Investigation; DDVallance: Methodology, Investigation, Visualization, Writing—Original Draft.

**Funding** Authors gratefully acknowledge the European Commission for funding the InnoRenew project (Grant agreement #739574 under the Horizon 2020 WIDESPREAD-2-Teaming program) and the Republic of Slovenia (investment funding from the Republic of Slovenia and the European Regional Development Fund), the European Union's Horizon 2020 research and innovation programme under the H2020 Marie Skłodowska-Curie Actions (Grant Number 898179), and COST Action CA17107.

**Data Availability** Not applicable.

**Code Availability** Not applicable.

## Declarations

**Conflict of interest** The authors declare that they have no conflict of interest.

**Open Access** This article is licensed under a Creative Commons Attribution 4.0 International License, which permits use, sharing, adaptation, distribution and reproduction in any medium or format, as long as you give appropriate credit to the original author(s) and the source, provide a link to the Creative Commons licence, and indicate if changes were made. The images or other third party material in this article are included in the article's Creative Commons licence, unless indicated otherwise in a credit line to the material. If material is not included in the article's Creative Commons licence and your intended use is not



permitted by statutory regulation or exceeds the permitted use, you will need to obtain permission directly from the copyright holder. To view a copy of this licence, visit <http://creativecommons.org/licenses/by/4.0/>.

## References






- Bouloc, P., Allegret, S., Arnaud, L., eds.: Hemp: Industrial Production and Uses. CABI, Wallingford, Oxfordshire (2013)
- Crini, G., Lichtfouse, E., Chanet, G., Morin-Crini, N.: Applications of hemp in textiles, paper industry, insulation and building materials, horticulture, animal nutrition, food and beverages, nutraceuticals, cosmetics and hygiene, medicine, agrochemistry, energy production and environment: a review. *Environ. Chem. Lett.* **18**, 1451–1476 (2020). <https://doi.org/10.1007/s10311-020-01029-2>
- Prade, T., Svensson, S.-E., Mattsson, J.E.: Energy balances for biogas and solid biofuel production from industrial hemp. *Biomass Bioenergy*. **40**, 36–52 (2012). <https://doi.org/10.1016/j.biombioe.2012.01.045>
- Prade, T., Finell, M., Svensson, S.-E., Mattsson, J.E.: Effect of harvest date on combustion related fuel properties of industrial hemp (*Cannabis sativa* L.). *Fuel* **102**, 592–604 (2012). <https://doi.org/10.1016/j.fuel.2012.05.045>
- Parvez, A.M., Lewis, J.D., Afzal, M.T.: Potential of industrial hemp (*Cannabis sativa* L.) for bioenergy production in Canada: status, challenges and outlook. *Renew. Sustain. Energy Rev.* **141**, 110784 (2021). <https://doi.org/10.1016/j.rser.2021.110784>
- Liu, Z., Balasubramanian, R.: Upgrading of waste biomass by hydrothermal carbonization (HTC) and low temperature pyrolysis (LTP): a comparative evaluation. *Appl. Energy*. **114**, 857–864 (2014). <https://doi.org/10.1016/j.apenergy.2013.06.027>
- Li, Q., Qi, J., Jiang, J., Wu, J., Duan, L., Wang, S., Hao, J.: Significant reduction in air pollutant emissions from household cooking stoves by replacing raw solid fuels with their carbonized products. *Sci. Total Environ.* **650**, 653–660 (2019). <https://doi.org/10.1016/j.scitotenv.2018.09.020>
- Khan, A.A., de Jong, W., Jansens, P.J., Spliethoff, H.: Biomass combustion in fluidized bed boilers: potential problems and remedies. *Fuel Process. Technol.* **90**, 21–50 (2009). <https://doi.org/10.1016/j.fuproc.2008.07.012>
- Nunes, L.J.R., Matias, J.C.O., Loureiro, L.M.E.F., Sá, L.C.R., Silva, H.F.C., Rodrigues, A.M., Causer, T.P., DeVallance, D.B., Ciolkosz, D.E.: Evaluation of the potential of agricultural waste recovery: energy densification as a factor for residual biomass logistics optimization. *Appl. Sci.* **11**, 20 (2021). <https://doi.org/10.3390/app11010020>
- Guo, M., Song, W., Buhain, J.: Bioenergy and biofuels: history, status, and perspective. *Renew. Sustain. Energy Rev.* **42**, 712–725 (2015). <https://doi.org/10.1016/j.rser.2014.10.013>
- Tsai, W.-T., Liu, S.-C., Hsieh, C.-H.: Preparation and fuel properties of biochars from the pyrolysis of exhausted coffee residue. *J. Anal. Appl. Pyrolysis*. **93**, 63–67 (2012). <https://doi.org/10.1016/j.jaap.2011.09.010>
- Basu, P.: Biomass Gasification Pyrolysis and Torrefaction. Elsevier, Amsterdam (2013)
- Liu, Z., Balasubramanian, R.: A comparison of thermal behaviors of raw biomass, pyrolytic biochar and their blends with lignite. *Bioresour. Technol.* **146**, 371–378 (2013). <https://doi.org/10.1016/j.biortech.2013.07.072>
- Liu, Z., Fei, B., Jiang, Z., Liu, X.: Combustion characteristics of bamboo-biochars. *Bioresour. Technol.* **167**, 94–99 (2014). <https://doi.org/10.1016/j.biortech.2014.05.023>
- Chin, K.L., H'ng, P.S., Go, W.Z., Wong, W.Z., Lim, T.W., Maminiski, M., Paridah, M.T., Luqman, A.C.: Optimization of torrefaction conditions for high energy density solid biofuel from oil palm biomass and fast growing species available in Malaysia. *Ind. Crops Prod.* **49**, 768–774 (2013). <https://doi.org/10.1016/j.indcrop.2013.06.007>
- Yousaf, B., Liu, G., Abbas, Q., Wang, R., Ubaid Ali, M., Ullah, H., Liu, R., Zhou, C.: Systematic investigation on combustion characteristics and emission-reduction mechanism of potentially toxic elements in biomass- and biochar-coal co-combustion systems. *Appl. Energy*. **208**, 142–157 (2017). <https://doi.org/10.1016/j.apenergy.2017.10.059>
- Zhang, C., Zeng, G., Huang, D., Lai, C., Chen, M., Cheng, M., Tang, W., Tang, L., Dong, H., Huang, B., Tan, X., Wang, R.: Biochar for environmental management: mitigating greenhouse gas emissions, contaminant treatment, and potential negative impacts. *Chem. Eng. J.* **373**, 902–922 (2019). <https://doi.org/10.1016/j.cej.2019.05.139>
- Wallace, C.A., Saha, G.C., Afzal, M.T., Lloyd, A.: Experimental and computational modeling of effective flexural/tensile properties of microwave pyrolysis biochar reinforced GFRP biocomposites. *Compos. Part B Eng.* **175**, 107180 (2019). <https://doi.org/10.1016/j.compositesb.2019.107180>
- Nan, N., DeVallance, D.B., Xie, X., Wang, J.: The effect of bio-carbon addition on the electrical, mechanical, and thermal properties of polyvinyl alcohol/biochar composites. *J. Compos. Mater.* **50**, 1161–1168 (2016). <https://doi.org/10.1177/0021998315589770>
- Shen, F., Luo, W., Dai, J., Yao, Y., Zhu, M., Hitz, E., Tang, Y., Chen, Y., Sprenkle, V.L., Li, X., Hu, L.: Ultra-thick, low-tortuosity, and mesoporous wood carbon anode for high-performance sodium-ion batteries. *Adv. Energy Mater.* **6**, 1600377 (2016). <https://doi.org/10.1002/aenm.201600377>
- Sun, W., Lipka, S.M., Swartz, C., Williams, D., Yang, F.: Hemp-derived activated carbons for supercapacitors. *Carbon* **103**, 181–192 (2016). <https://doi.org/10.1016/j.carbon.2016.02.090>
- Teng, S., Siegel, G., Wang, W., Tiwari, A.: Carbonized wood for supercapacitor electrodes. *ECS Solid State Lett.* **3**, M25 (2014). <https://doi.org/10.1149/2.005405ssl>
- Nan, N., DeVallance, D.B.: Development of poly(vinyl alcohol)/wood-derived biochar composites for use in pressure sensor applications. *J. Mater. Sci.* **52**, 8247–8257 (2017). <https://doi.org/10.1007/s10853-017-1040-7>
- Rowell, R.M., Pettersen, R., Tshabalala, M.A.: Chapter 3 cell wall chemistry. In: *Handbook Wood Chem. Wood Compos.*, 2nd Ed., pp 33–72 (2013), 3, 33–72 (2012)
- Elaieb, M.T., Khouaja, A., Khouja, M.L., Valette, J., Volle, G., Candelier, K.: Comparative study of local Tunisian woods properties and the respective qualities of their charcoals produced by a new industrial eco-friendly carbonization process. *Waste Biomass Valorization*. **9**, 1199–1211 (2018). <https://doi.org/10.1007/s12649-016-9780-1>
- CEN/TS 14918:2005—Solid biofuels—method for the determination of calorific value. (2005)
- Marinho, B., Ghislandi, M., Tkalya, E., Koning, C.E., de With, G.: Electrical conductivity of compacts of graphene, multi-wall carbon nanotubes, carbon black, and graphite powder. *Powder Technol.* **221**, 351–358 (2012). <https://doi.org/10.1016/j.powtec.2012.01.024>
- Gandolfi, S., Ottolina, G., Riva, S., Fantoni, G.P., Patel, I.: Complete chemical analysis of Carmagnola hemp hurds and structural features of its components. *BioResources* **8**, 2641–2656 (2013)

29. Xie, C., Gong, W., Yang, Q., Zhu, Z., Yan, L., Hu, Z., Peng, Y.: White-rot fungi pretreatment combined with alkaline/oxidative pretreatment to improve enzymatic saccharification of industrial hemp. *Bioresour. Technol.* **243**, 188–195 (2017). <https://doi.org/10.1016/j.biortech.2017.06.077>
30. Ji, A., Jia, L., Kumar, D., Yoo, C.G.: Recent advancements in biological conversion of industrial hemp for biofuel and value-added products. *Fermentation*. **7**, 6 (2021). <https://doi.org/10.3390/fermentation7010006>
31. Gutiérrez, A., Rodríguez, I.M., del Río, J.C.: Chemical characterization of lignin and lipid fractions in industrial hemp bast fibers used for manufacturing high-quality paper pulps. *J. Agric. Food Chem.* **54**, 2138–2144 (2006). <https://doi.org/10.1021/jf052935a>
32. Cigasova, J., Stevulova, N., Schwarzova, I., Junak, J.: Innovative use of biomass based on technical hemp in building industry. *Chem. Eng. Trans.* **37**, 685–690 (2014). <https://doi.org/10.3303/CET1437115>
33. Burhenne, L., Messmer, J., Aicher, T., Laborie, M.-P.: The effect of the biomass components lignin, cellulose and hemicellulose on TGA and fixed bed pyrolysis. *J. Anal. Appl. Pyrolysis*. **101**, 177–184 (2013). <https://doi.org/10.1016/j.jaap.2013.01.012>
34. Demirbaş, A.: Relationships between lignin contents and heating values of biomass. *Energy Convers. Manag.* **42**, 183–188 (2001). [https://doi.org/10.1016/S0196-8904\(00\)00050-9](https://doi.org/10.1016/S0196-8904(00)00050-9)
35. Angelini, L., Tavarini, S.B.C., Beni, C.: Variation in mineral composition in three different plant organs of five fibre hemp (*Cannabis sativa* L.) cultivars. *Agrochimica* **58**, 1–18 (2014)
36. Raveendran, K., Ganesh, A., Khilar, K.C.: Pyrolysis characteristics of biomass and biomass components. *Fuel* **75**, 987–998 (1996). [https://doi.org/10.1016/0016-2361\(96\)00030-0](https://doi.org/10.1016/0016-2361(96)00030-0)
37. Yang, H., Yan, R., Chen, H., Lee, D.H., Zheng, C.: Characteristics of hemicellulose, cellulose and lignin pyrolysis. *Fuel* **86**, 1781–1788 (2007). <https://doi.org/10.1016/j.fuel.2006.12.013>
38. Williams, P.T., Besler, S.: Thermogravimetric analysis of the components of biomass. In: Bridgwater, A.V. (ed.) *Advances in Thermochemical Biomass Conversion*, pp. 771–783. Springer, Dordrecht (1993)
39. Miranda, T., Montero, I., Sepúlveda, F.J., Arranz, J.I., Rojas, C.V., Nogales, S.: A review of pellets from different sources. *Materials*. **8**, 1413–1427 (2015). <https://doi.org/10.3390/ma8041413>
40. Obernberger, I., Thek, G.: Physical characterisation and chemical composition of densified biomass fuels with regard to their combustion behaviour. *Biomass Bioenergy*. **27**, 653–669 (2004). <https://doi.org/10.1016/j.biombioe.2003.07.006>
41. Askeland, M., Clarke, B., Paz-Ferreiro, J.: Comparative characterization of biochars produced at three selected pyrolysis temperatures from common woody and herbaceous waste streams. *PeerJ* **7**, e6784 (2019). <https://doi.org/10.7717/peerj.6784>
42. Leng, L., Yang, L., Leng, S., Zhang, W., Zhou, Y., Peng, H., Li, H., Hu, Y., Jiang, S., Li, H.: A review on nitrogen transformation in hydrochar during hydrothermal carbonization of biomass containing nitrogen. *Sci. Total Environ.* **756**, 143679 (2021). <https://doi.org/10.1016/j.scitotenv.2020.143679>
43. Toor, S.S., Rosendahl, L., Rudolf, A.: Hydrothermal liquefaction of biomass: a review of subcritical water technologies. *Energy* **36**, 2328–2342 (2011). <https://doi.org/10.1016/j.energy.2011.03.013>
44. Li, Y., Liu, H., Xiao, K., Liu, X., Hu, H., Li, X., Yao, H.: Correlations between the physicochemical properties of hydrochar and specific components of waste lettuce: influence of moisture, carbohydrates, proteins and lipids. *Bioresour. Technol.* **272**, 482–488 (2019). <https://doi.org/10.1016/j.biortech.2018.10.066>
45. Wyn, H.K., Zárate, S., Carrascal, J., Yermán, L.: A novel approach to the production of biochar with improved fuel characteristics from biomass waste. *Waste Biomass Valorization*. **11**, 6467–6481 (2020). <https://doi.org/10.1007/s12649-019-00909-1>
46. Shafizadeh, F.: Pyrolytic reactions and products of biomass. In: Overend, R.P., Milne, T.A., Mudge, L.K. (eds.) *Fundamentals of Thermochemical Biomass Conversion*, pp. 183–217. Springer, Dordrecht (1985)
47. Kraszkiewicz, A., Kachel, M., Parafiniuk, S., Zając, G., Niedziółka, I., Sprawka, M.: Assessment of the possibility of using hemp biomass (*Cannabis sativa* L.) for energy purposes: a case study. *Appl. Sci.* **9**, 4437 (2019). <https://doi.org/10.3390/app9204437>
48. Wallace, C.A., Afzal, M.T., Saha, G.C.: Effect of feedstock and microwave pyrolysis temperature on physio-chemical and nano-scale mechanical properties of biochar. *Bioresour. Bioprocess.* **6**, 33 (2019). <https://doi.org/10.1186/s40643-019-0268-2>
49. Branca, C., Di Blasi, C., Galgano, A.: Experimental analysis about the exploitation of industrial hemp (*Cannabis sativa*) in pyrolysis. *Fuel Process. Technol.* **162**, 20–29 (2017). <https://doi.org/10.1016/j.fuproc.2017.03.028>
50. Sun, J., Shen, Z., Zhang, Y., Zhang, Q., Wang, F., Wang, T., Chang, X., Lei, Y., Xu, H., Cao, J., Zhang, N., Liu, S., Li, X.: Effects of biomass briquetting and carbonization on PM<sub>2.5</sub> emission from residential burning in Guanzhong Plain, China. *Fuel* **244**, 379–387 (2019). <https://doi.org/10.1016/j.fuel.2019.02.031>
51. Mermoud, F., Salvador, S., Van de Steene, L., Golfier, F.: Influence of the pyrolysis heating rate on the steam gasification rate of large wood char particles. *Fuel* **85**, 1473–1482 (2006). <https://doi.org/10.1016/j.fuel.2005.12.004>
52. Chaves Fernandes, B.C., Ferreira Mendes, K., Dias Júnior, A.F., da Silva Caldeira, V.P., da Silva Teófilo, T.M., Severo Silva, T., Mendonça, V., de Freitas Souza, M., Valadão Silva, D.: Impact of pyrolysis temperature on the properties of eucalyptus wood-derived biochar. *Materials*. (2020). <https://doi.org/10.3390/ma13245841>
53. Keilueit, M., Nico, P.S., Johnson, M.G., Kleber, M.: Dynamic molecular structure of plant biomass-derived black carbon (biochar). *Environ. Sci. Technol.* **44**, 1247–1253 (2010). <https://doi.org/10.1021/es9031419>
54. Yuan, H., Lu, T., Huang, H., Zhao, D., Kobayashi, N., Chen, Y.: Influence of pyrolysis temperature on physical and chemical properties of biochar made from sewage sludge. *J. Anal. Appl. Pyrolysis*. **112**, 284–289 (2015). <https://doi.org/10.1016/j.jaap.2015.01.010>
55. Raveendran, K., Ganesh, A.: Heating value of biomass and biomass pyrolysis products. *Fuel* **75**, 1715–1720 (1996). [https://doi.org/10.1016/S0016-2361\(96\)00158-5](https://doi.org/10.1016/S0016-2361(96)00158-5)
56. Demirbaş, P.A.: Fuel and combustion properties of bio-wastes. *Energy Sources* **27**, 451–462 (2005). <https://doi.org/10.1080/00908310490441863>
57. Ronse, F., van Hecke, S., Dickinson, D., Prins, W.: Production and characterization of slow pyrolysis biochar: influence of feedstock type and pyrolysis conditions. *GCB Bioenergy*. **5**, 104–115 (2013). <https://doi.org/10.1111/gcbb.12018>
58. Shao, Y., Guizani, C., Grosseau, P., Chaussy, D., Beneventi, D.: Biocarbons from microfibrillated cellulose/lignosulfonate precursors: a study of electrical conductivity development during slow pyrolysis. *Carbon* **129**, 357–366 (2018). <https://doi.org/10.1016/j.carbon.2017.12.037>
59. McDonald-Wharry, J., Manley-Harris, M., Pickering, K.: Carbonisation of biomass-derived chars and the thermal reduction of a graphene oxide sample studied using Raman spectroscopy. *Carbon* **59**, 383–405 (2013). <https://doi.org/10.1016/j.carbon.2013.03.033>
60. Peng, W., Li, H., Hu, Y., Liu, Y., Song, S.: Characterisation of reduced graphene oxides prepared from natural flaky, lump and amorphous graphites. *Mater. Res. Bull.* **78**, 119–127 (2016). <https://doi.org/10.1016/j.materresbull.2016.02.034>

61. Escribano, R., Sloan, J.J., Siddique, N., Sze, N., Dudev, T.: Raman spectroscopy of carbon-containing particles. *Vib. Spectrosc.* **26**, 179–186 (2001). [https://doi.org/10.1016/S0924-2031\(01\)00106-0](https://doi.org/10.1016/S0924-2031(01)00106-0)
62. McCulloch, D.G., Prawer, S., Hoffman, A.: Structural investigation of xenon-ion-beam-irradiated glassy carbon. *Phys. Rev. B.* **50**, 5905–5917 (1994). <https://doi.org/10.1103/PhysRevB.50.5905>
63. Li, X., Hayashi, J., Li, C.-Z.: FT-Raman spectroscopic study of the evolution of char structure during the pyrolysis of a Victorian brown coal. *Fuel* **85**, 1700–1707 (2006). <https://doi.org/10.1016/j.fuel.2006.03.008>
64. Contreras, R.C., Guicheret, B., Machado, B.F., Rivera-Cárcamo, C., Curiel Alvarez, M.A., Valdez Salas, B., Rutttert, M., Placke, T., Favre Réguiillon, A., Vanoye, L., de Bellefon, C., Philippe, R., Serp, P.: Effect of mesoporous carbon support nature and pretreatments on palladium loading, dispersion and apparent catalytic activity in hydrogenation of myrcene. *J. Catal.* **372**, 226–244 (2019). <https://doi.org/10.1016/j.jcat.2019.02.034>
65. Tzeng, S.-S., Pan, J.-H.: Oxidative stabilization of petroleum pitch at high pressure and its effects on the microstructure and carbon yield after carbonization/graphitization. *Mater. Chem. Phys.* **74**, 214–221 (2002). [https://doi.org/10.1016/S0254-0584\(01\)00468-0](https://doi.org/10.1016/S0254-0584(01)00468-0)
66. del Corro, E., de la Roza, A.O., Taravillo, M., Baonza, V.G.: Raman modes and Grüneisen parameters of graphite under compressive biaxial stress. *Carbon* **50**, 4600–4606 (2012). <https://doi.org/10.1016/j.carbon.2012.05.046>
67. Harris, P.J.F., Liu, Z., Suenaga, K.: Imaging the atomic structure of activated carbon. *J. Phys. Condens. Matter.* **20**, 362201 (2008). <https://doi.org/10.1088/0953-8984/20/36/362201>

**Publisher's Note** Springer Nature remains neutral with regard to jurisdictional claims in published maps and institutional affiliations.

## Authors and Affiliations

Laetitia Marrot<sup>1,2</sup>  · Kevin Candelier<sup>3,4</sup>  · Jérémy Valette<sup>3,4</sup> · Charline Lanvin<sup>3,4</sup> · Barbara Horvat<sup>5</sup>  · Lea Legan<sup>6</sup>  · David B. DeVallance<sup>1,2</sup> 

Kevin Candelier  
kevin.candelier@cirad.fr

Jérémy Valette  
jeremy.valette@cirad.fr

Charline Lanvin  
charline.lanvin@cirad.fr

Barbara Horvat  
barbara.horvat@zag.si

Lea Legan  
lea.legan@zvks.si

David B. DeVallance  
devallance@innorenew.eu

<sup>2</sup> Andrej Marušič Institute, University of Primorska, Muzejski trg 2, 6000 Koper, Slovenia

<sup>3</sup> CIRAD, Research Unit BioWooEB, 34000 Montpellier, France

<sup>4</sup> BioWooEB, Université de Montpellier, CIRAD, Montpellier, France

<sup>5</sup> Slovenian National Building and Civil Engineering Institute, Dimičeva ulica 12, 1000 Ljubljana, Slovenia

<sup>6</sup> Institute for the Protection of Cultural Heritage of Slovenia, Poljanska 40, 1000 Ljubljana, Slovenia

<sup>1</sup> InnoRenew CoE, Livade 6, 6310 Izola, Slovenia